

Universality classes of transition fronts in the FPU model

N.Gorbushin,¹ A. Vainchtein,² and L. Truskinovsky¹

¹*PMMH, CNRS – UMR 7636, CNRS, ESPCI Paris, PSL Research University, 10 rue Vauquelin, 75005 Paris, France*

²*Department of Mathematics, University of Pittsburgh, Pittsburgh, Pennsylvania 15260, USA*

(Dated: April 13, 2021)

Steady transition fronts in nonlinear lattices are among the most important dynamic coherent structures. We use the Fermi-Pasta-Ulam model with piecewise linear nonlinearity to show that there are exactly three distinct classes of such fronts which differ fundamentally in how (and whether) they produce and transport oscillations. To make this Hamiltonian problem analytically transparent, we construct a quasicontinuum approximation generating all three types of fronts and then show that the interconnection between different classes of fronts in the original discrete model is the same as in the quasicontinuum model. The proposed framework unifies previous attempts to classify the transition fronts as radiative, dispersive, topological or compressive and categorizes them instead as different types of dynamic defects.

Dynamic switching fronts in discrete systems are highly nonlinear far-from equilibrium coherent structures playing an important role in the energy transmission from macro to microscales. They are observed in both integrable and non-integrable Hamiltonian systems [1, 2], can be topological or non-topological [3–5], spreading or compact [6], compressive or undercompressive (non-Lax) [7], stable or unstable [8]. Together with solitons and breathers, they play a crucial role as building blocks in complex nonlinear wave patterns emerging generically in mechanical systems ranging from crystals [9–11], and metamaterials [12–15] to nanomechanical systems [13, 16–18]. Similar concepts have been applied to describe transport properties of many nonmechanical dispersive systems as well [19–23].

Despite the ubiquity of transition fronts, the relation between different *classes* of such mobile nonlinear structures remains obscure. In this Letter we take a well known prototypical system, the Fermi-Pasta-Ulam (FPU) model [24, 25] and present a unifying description of the three main types of transition fronts which we identify as *subkinks*, *shocks* and *superkinks*. All of them have been previously treated as mostly unrelated: subkinks as subsonic phase boundaries [26], shocks as classical supersonic shock waves [27, 28] and superkinks as supersonic activity waves [29]. To identify the universality classes of such localized flow defects, we use the simplest choice of nonlinearity by assuming that the interactions are piecewise linear. Such interactions were introduced in the original FPU paper [24] and have since been employed for the description of various dynamic nonlinear phenomena, e.g. [30–32].

To make the problem amenable to analytic study, we first construct a quasicontinuum (QC) version of the FPU system, which is compatible with all three types of fronts. It can be viewed as a higher order version of the ‘good’ Boussinesq approximation which keeps the elastic energy local but focuses instead on the nonlocality of the kinetic energy [33]. In this simplified framework it becomes transparent, for instance, why some kinks are radiative and others are not, and why some shocks are dispersive, while others are not. We then return to the original discrete (D) system and obtain a general traveling wave solution of the piecewise linear FPU system, which incorporates as special cases all three types of fronts.

We show that the interrelation between different classes of transition fronts in the D and QC models is exactly the same.

We recall that the FPU system describes the Hamiltonian dynamics of a mass-spring chain with mass displacements $u_n(t)$ satisfying a potentially infinite system of equations

$$\rho h \frac{d^2 u_n(t)}{dt^2} = \sigma \left(\frac{u_{n+1} - u_n}{h} \right) - \sigma \left(\frac{u_n - u_{n-1}}{h} \right), \quad (1)$$

where h is the equilibrium distance between the masses $m = \rho h$, where ρ is the mass density. In terms of the strain variables $\varepsilon_n(t) = (u_{n+1}(t) - u_n(t))/h$ the piecewise linear macroscopic stress-strain relation can be written as $\sigma(\varepsilon) = E_1 \varepsilon$, for $\varepsilon < \varepsilon_c$ and $\sigma(\varepsilon) = E_2 \varepsilon - \sigma_0$ for $\varepsilon > \varepsilon_c$, where ε_c is the critical (switching) strain and $E_2 > E_1$ are the elastic moduli of the two ‘phases’. The stress jump at the critical strain, ensuring continuity of the piecewise quadratic elastic energy, is $\Delta\sigma = \sigma_0 - (E_2 - E_1)\varepsilon_c$, which may vary from positive to negative.

As we vary the parameter $\Delta\sigma$ and the velocity of the front, we obtain three types of transitions: subkinks (subsonic kinks), intersonic shocks and superkinks (supersonic kinks), shown schematically in panels (a), (b) and (c) of Fig. 1. They were first formally identified as separate solutions in [32, 34], and the goal of the paper is to reveal their interconnections in the framework of the FPU model.

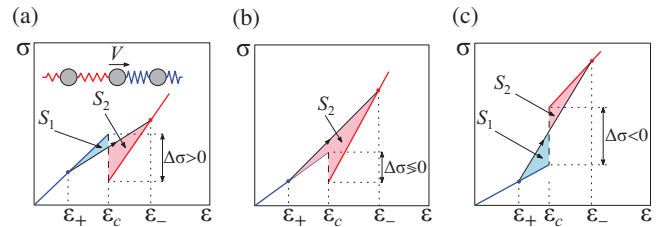


Figure 1. Distinct cases of traveling wave solutions: (a) subsonic kinks, $V < c_1 < c_2$, (b) shocks, $c_1 < V < c_2$, (c) supersonic kinks, $c_1 < c_2 < V$. The driving force is $G = S_2 - S_1$, where $S_{1,2}$ are the areas cut by the Rayleigh line $\rho V^2 = (\sigma(\varepsilon_+) - \sigma(\varepsilon_-))/(\varepsilon_+ - \varepsilon_-)$.

Numerical simulations show stable propagation of all three types of transition waves; see Fig. 2. If the constant velocity of the front is V , we find that the subkinks exist when

$V < c_1 < c_2$ (Fig. 2(a)), shocks when $c_1 < V < c_2$ (Fig. 2(b,c)) and superkinks when $c_1 < c_2 < V$ (Fig. 2(d)), where $c_{1,2} = \sqrt{E_{1,2}/\rho}$ are two characteristic speeds. Note that in the case of shocks we observe different behaviors depending on the value of $\Delta\sigma$: either a traveling wave with stationary profile (Fig. 2(b)) or a dispersive shock profile with spreading profile (Fig. 2(c)). Some links between subkinks and shocks were established in [27, 28], while superkinks remain so far a disconnected class of transition fronts [29, 35].

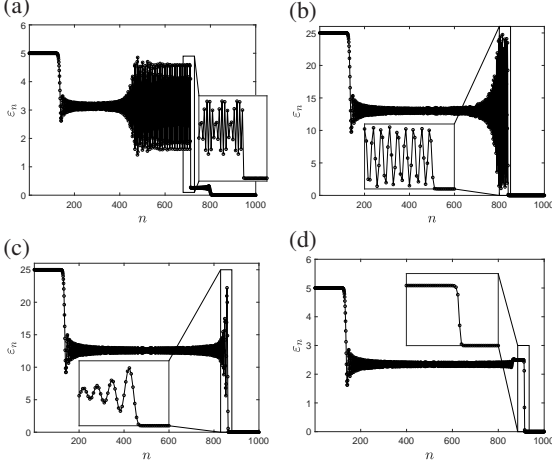


Figure 2. Different regimes of front propagation initiated by Riemann-type initial conditions with different left strain ε_l and $\Delta\sigma$: (a) subkink ($\varepsilon_l = 5$, $\Delta\sigma = 2.5$); (b) conventional shock ($\varepsilon_l = 25$, $\Delta\sigma = 2.5$); (c) dispersive shock ($\varepsilon_l = 25$, $\Delta\sigma = 0$); (d) superkink ($\varepsilon_l = 5$, $\Delta\sigma = -1.5$). Here $E_1 = 1$, $E_2 = 1.5$, $\rho = 1$, $h = 1$, $\varepsilon_c = 1$ and $t = 300$.

To obtain a unified description of all these types of transition waves, we first turn to the classical continuum limit $h \rightarrow 0$. This yields the nonlinear wave equation, which can be represented as the first-order system $\varepsilon_t = v_x$, $\rho v_t = \sigma_x$, where $\varepsilon(x, t) = u_x$ and $v(x, t) = u_t$ are the strain and particle velocity, respectively. This system has discontinuous solutions which satisfy Rankine-Hugoniot (RH) conditions $[[v]] + V[[\varepsilon]] = 0$, $\rho V[[v]] + [[\sigma(\varepsilon)]] = 0$, where $[[f]] \equiv f_+ - f_-$ is the jump between the values on the right and on the left and V is the velocity of the front.

There are five variables to be determined: v_{\pm} , ε_{\pm} and V ; see Fig.1. Due to piecewise linearity, two characteristics with velocities $\pm c_{1,2}$ can be defined on both sides of the jump. Fig. 3 shows the actual arrangement of characteristics for subkinks ($V < c_1$), shocks ($c_1 < V < c_2$) and superkinks ($V > c_2$). If $V < c_1$ or $V > c_2$ there are two incoming characteristics on the front which reduces the number of unknowns to one and therefore an additional condition is needed to find V . If $c_1 < V < c_2$, there are three incoming characteristics, and no additional conditions are needed. In this sense kinks are undercompressive (non-Lax), while shocks are compressive.

The scale-free approximation adopted in continuum mechanics does not reveal why an additional macroscopic condition is needed in the case of subkinks and superkinks and why the case of shocks has to be subdivided into two sub-cases, as suggested by our simulation results. To this end

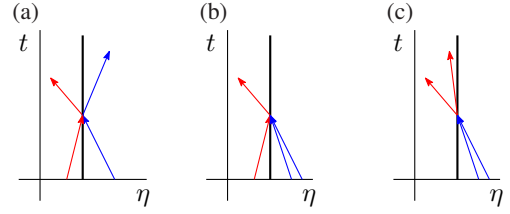


Figure 3. Characteristics $\eta \pm (c_{1,2} \pm V)t = \text{const}$ of the continuum problem in the moving frame with $\eta = x - Vt$ in phase 1 (blue) and phase 2 (red): (a) subkinks, $V < c_1$; (b) shocks, $c_1 < V < c_2$; (c) superkinks, $V > c_2$. Here $\eta = x - Vt$.

we need a QC approximation carrying internal length and/or time scales [36, 37]. Following the arguments in [33], we choose to work with internal time scales and build upon the approach proposed in [38, 39]. Setting $x = nh$, $\varepsilon_n(t) = \varepsilon(x, t)$ and $\sigma(\varepsilon_n(t)) = \sigma(x, t)$, one can rewrite the equations of motion as an advance-delay differential equation for $\varepsilon(x, t)$, which in Fourier space is given by $\rho h^2 d^2 \hat{\varepsilon} / dt^2 = -\sin^2(kh/2) \hat{\sigma}$, where $\hat{f}(k, t) = \int_{-\infty}^{\infty} f(x, t) \exp(ikx) dx$. Using the Padé approximation $4 \sin^2(kh/2) \approx (kh)^2 / (1 + a_1(kh)^2 + a_2(kh)^4)$, where $a_1 = 1/12$ and $a_2 = 1/240$, and then transforming back to physical space, we find that in our QC approximation of the FPU system the displacement field $u(x, t)$ is governed by

$$\rho \left(1 - a_1 \frac{\partial^2}{\partial x^2} + a_2 \frac{\partial}{\partial x^4} \right) \frac{d^2 u}{dt^2} = \frac{\partial \sigma}{\partial x} \quad (2)$$

where we used the scaling $\tilde{x} = x/h$ but dropped the tildes. This equation can be also obtained from the Hamiltonian principle with kinetic energy density $(\rho/2)(u_t^2 + a_1(u_{tx})^2 + a_2(u_{txx})^2)$ and potential energy density $\phi(u_x) = (E_1/2)u_x^2$ for $u_x < \varepsilon_c$ and $\phi(u_x) = (E_2/2)(u_x^2 - \varepsilon_c^2) - \sigma_0(u_x - \varepsilon_c) + (E_1/2)\varepsilon_c^2$ for $u_x > \varepsilon_c$. The same variational principle can be used to obtain jump conditions at $u_x = \varepsilon_c$.

Indeed, consider the action functional of the form $\mathcal{A} = \int_{\Omega} \mathcal{L}(u_{,i}, u_{,ij}, u_{,ijk}) dq^1 dq^2$, where $q^1 = x$, $q^2 = t$, subscripts after comma indicate partial derivatives and $\mathcal{L} = (\rho/2)(u_t^2 + a_1 u_{tx}^2 + a_2 u_{txx}^2) - \phi(u_x)$. The integration is over a two-dimensional space-time domain Ω . The corresponding Euler-Lagrange equation $\partial_i (\partial \mathcal{L} / \partial u_{,i}) - \partial_j (\partial \mathcal{L} / \partial u_{,ij}) + \partial_{jk} (\partial \mathcal{L} / \partial u_{,ijk}) = 0$ coincides with Eq. (2). Consider a propagating jump surface Γ where $[[u]] = 0$. On such broken extremal the action principle imposes the following dispersive RH (DRH) conditions[40]: $[[\partial \mathcal{L} / \partial u_{,i} - \partial_j (\partial \mathcal{L} / \partial u_{,ij}) + \partial_{jk} (\partial \mathcal{L} / \partial u_{,ijk})]] n_i = 0$, $[[\partial \mathcal{L} / \partial u_{,ij} - \partial_k (\partial \mathcal{L} / \partial u_{,ijk})]] n_i n_j = 0$ and $[[\partial \mathcal{L} / \partial u_{,ijk}]] n_i n_j n_k = 0$. Here n_a is a normal vector to Γ , so $n_2 = -n_1 V$. The kinematic compatibility conditions $[[u_{,i}]] = \mu n_i$, where μ is a scalar, represent the mass balance $V[[u_{,1}]] + [[u_{,2}]] = 0$.

In what follows, we use dimensionless variables $\tilde{V} = V/c_1$, $\tilde{\sigma} = \sigma/E_1$, $\tilde{\sigma}_0 = \sigma_0/E_1$ but drop the tildes. We also introduce the main dimensionless parameter $\gamma^2 = E_2/E_1 > 1$. To find steadily moving transition fronts, we seek solutions of

Eq. (2) in the form of traveling waves $\varepsilon(x, t) = \varepsilon(\eta)$, where $\eta = x - Vt$. If we place the front at $\eta = 0$ we must require that the *consistency* condition $\varepsilon(0) = \varepsilon_c$ is satisfied. We also need to apply the boundary conditions $\langle \varepsilon(\eta) \rangle \rightarrow \varepsilon_{\pm}$ as $\eta \rightarrow \pm\infty$ with constant limits ε_{\pm} , where the angular brackets denote the average over the short-wave oscillations.

Integrating (2) twice and taking into account the boundary conditions we obtain the traveling wave equation

$$V^2 \left[1 - a_1 \frac{d^2}{d\eta^2} + a_2 \frac{d^4}{d\eta^4} \right] \varepsilon(\eta) = \sigma(\eta) + (V^2 - 1)\varepsilon_+, \quad (3)$$

where $\sigma(\eta) = \varepsilon(\eta)H(\eta) + (\gamma\varepsilon(\eta) - \sigma_0)H(-\eta)$. Since Eq. (3) is piecewise linear, it can be solved explicitly in terms of four nonzero roots of each of the characteristic equations $\omega_{\pm}(k) = kV$, where $\omega_{+}^2(k)/k^2 = \omega_{-}^2(k)/(\gamma k)^2 = (1 + a_1 k^2 + a_2 k^4)^{-1}$ are the dispersion relations in the two linear regimes. For simplicity, we assume that $\gamma < \sqrt{12/7}$ and $V < \sqrt{12/7}$ in what follows (see [41] for the general case). Of particular importance are nonzero real roots, which correspond to energy radiation (see Fig. 4). A single symmetric pair $\pm k^{\pm}$

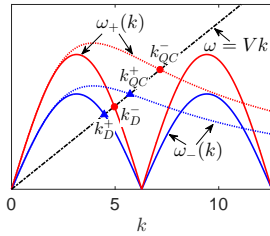


Figure 4. Comparison of the dispersion relations (for real k) in D (solid lines) and QC (dotted lines) models. In the picture the characteristic equations for D and QC models have one positive real root each, denoted by k_{QC}^{\pm} and k_D^{\pm} , respectively.

of such roots exists on each side when $V < 1$ (subkinks). When $1 < V < \gamma$ (shocks), only $\pm k^-$ remain, and in the case of superkinks there are no nonzero real roots. The other nonzero roots are purely imaginary and symmetric about the real axis. To find the coefficients associated with the different exponents, we need to apply at $\eta = 0$ the *continuity* conditions $[[\varepsilon]] = [[d\varepsilon/d\eta]] = 0$, together with the DRH conditions $a_1 [[d\varepsilon/d\eta]] = a_2 [[d^3\varepsilon/d\eta^3]]$ and $[[d^2\varepsilon/d\eta^2]] = 0$. To exclude the energy flux from infinity, we must also impose the *radiation* conditions $\omega'_+(k) > kV$ and $\omega'_-(k) < kV$ for positive real roots of the corresponding characteristic equations. The resulting solutions have the form

$$\varepsilon(\eta) = \varepsilon_{\pm} + \Lambda_{\pm}(\eta) + \Phi_{\pm}(\eta), \quad \eta \gtrless 0, \quad (4)$$

Here the limiting values of strain ε_{\pm} at $\eta \rightarrow \pm\infty$ satisfy the RH condition $V^2 = (\sigma(\varepsilon_+) - \sigma(\varepsilon_-))/(\varepsilon_+ - \varepsilon_-)$. Excluding the flux from infinity, we find that the radiation component of the solution is zero ahead of the front in all three cases: $\Lambda_+ \equiv 0$. Behind the front, it has the form

$$\Lambda_-(\eta) = 2\alpha^- \cos(k^-\eta + \beta^-) \quad (5)$$

for subkinks and shocks and equals zero for superkinks. The third term Φ_{\pm} in Eq. (4) describes the exponentially localized boundary layers and involves a single exponent on each side for subkinks and behind the front for shocks, while in the other cases there are two exponential terms [41]. Together with Eq. (5) and consistency condition, this implies that in the range $V < 1$ (subkinks) there is one unknown coefficient on + side and three on - side. All of them can be found from the four continuity/DRH conditions. When $1 < V < \gamma$ (shocks) we have two coefficients on + side and three on - side, and four conditions leave one of the constants *undetermined*. Finally, if $V > \gamma$ (superkinks) there are two coefficients on each side, so the solution is again fully specified by the four conditions [41].

The physical nature of the transition fronts in Eq. (4) is revealed by the structure of the roots of the characteristic equations, which describe the asymptotic behavior of the heteroclinic trajectories at $\eta \rightarrow \pm\infty$. Thus, for $V < 1$ (subkinks) the (non-generic) transition fronts correspond to center-saddle to a center-saddle trajectories; such transitions are possible due to the higher order dispersion included into our QC model. For $1 < V < \gamma$ (shocks) the heteroclinic orbits are generic saddle-saddle to center-saddle. Finally, for $\gamma < V$ (superkinks) the transitions are (non-generic) saddle-saddle to saddle-saddle connections.

Additional insights can be obtained by looking at the energy balance in the three classes of fronts. According to a continuum model the rate of energy dissipation on a front is $\mathcal{R} = GV \geq 0$, where $G = [[\phi(\varepsilon)]] - \{\sigma(\varepsilon)\} [[\varepsilon]]$, where $\{f\} = (f_+ + f_-)/2$ [26, 42]. In our case G can be computed explicitly:

$$G = \frac{\gamma^2 - 1}{2} (\varepsilon_+ \varepsilon_- - \varepsilon_c^2) + \frac{\sigma_0}{2} (\varepsilon_+ + \varepsilon_- - 2\varepsilon_c). \quad (6)$$

In the QC setting this energy does not disappear but is transferred, in the case of subkinks and shocks, at the relative velocity $\omega'_-(k^-) - V$ into a short-length wave (with wave number k^-) carrying it away from the front and propagating behind it. This yields $\mathcal{R} = \mathcal{R}_+ + \mathcal{R}_-$, where $\mathcal{R}_{\pm} = G_{\pm}V$, with $G_+ = 0$ (no radiation ahead) for all three types of fronts,

$$G_- = 2\gamma^2(\alpha^-)^2 \left(1 - \frac{\omega'_-(k^-)}{V} \right)$$

for $V < \gamma$ (subkinks and shocks) and $G_- = 0$ for superkinks.

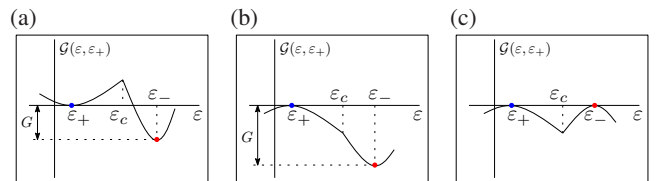


Figure 5. Different behavior of the dissipation function $\mathcal{G}(\varepsilon, \varepsilon_+)$: (a) subsonic kinks, $V < 1$, (b) shocks, $1 < V < \gamma$, (c) supersonic kinks, $V > \gamma$.

Further physical intuition can be developed if for all three classes of fronts we consider the function $\mathcal{G}(\varepsilon, \varepsilon_+) = \phi(\varepsilon) -$

$\phi(\varepsilon_+) - \Sigma(\varepsilon - \varepsilon_+)$, where $\Sigma(\varepsilon) = \sigma(\varepsilon_+) + (V^2/2)(\varepsilon - \varepsilon_+)$, introduced in [43]. It represents energy variation along the Rayleigh line which ensures the conservation of the macroscopic mass and momentum and the reference is chosen so that $\mathcal{G}(\varepsilon_+, \varepsilon_+) = 0$ and $\mathcal{G}(\varepsilon_+, \varepsilon_-) = -G \leq 0$. As we see in Fig. 5, for subkinks, in addition to dissipation, there is a barrier that needs to be overcome and the required energy is transmitted by dispersion from downstream. For shocks, there is no barrier but there is dissipation. Finally, for superkinks, there is no dissipation, but there is an anti-barrier and energy transfer by dispersion is still necessary, but now from upstream. Since the barriers exist in the case of kinks and not shocks, the former are topological, while the latter are non-topological flow defects.

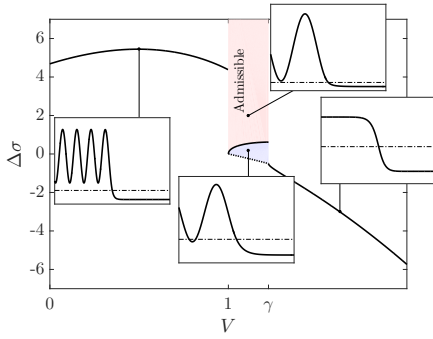


Figure 6. Admissibility sets of solutions of the QC problems. In the blue region we observe $\varepsilon(\eta) \leq \varepsilon_c$ when $\eta < \varepsilon_c$, and the dashed curves mark the threshold $\varepsilon_- = \varepsilon_c$. The insets show examples of the strains $\varepsilon(\eta)$. Here $\gamma^2 = 1.5$, $\varepsilon_c = 1$, and we set $\varepsilon_+ = 0$ for shock solutions. The corresponding diagram for the D problem is shown in [41].

The condition of admissibility for the obtained solutions takes the form $\varepsilon(\eta) > \varepsilon_c$ for $\eta < 0$ and $\varepsilon(\eta) < \varepsilon_c$ for $\eta > 0$. Fig. 6 shows that only some of the stationary shock solutions are admissible in the QC problem, which agrees with the numerical results for the D model in Fig. 2. Numerical simulations for the QC model show that in the domain of non-admissibility stationary shocks are replaced by spreading dispersive shock waves (DSW) [41]. This result, known for the D model with convex energy (our $\Delta\sigma \leq 0$), was previously linked to the low dimensionality and the absence of dissipation [44]. By allowing regimes with $\Delta\sigma \geq 0$, we recover the stationary shocks, because due to non-convexity, large-amplitude lattice waves, transmitting radiated energy away from the moving front, can now be accommodated.

The bilinear nature of the stress-strain relation allows one to find explicit representations for all three classes of fronts also in the D problem. To find traveling waves in this case, we need to solve the equation

$$V^2 \frac{d^2 \varepsilon}{d\eta^2} = \sigma(\eta + 1) + \sigma(\eta - 1) - 2\sigma(\eta). \quad (7)$$

where $\sigma(\eta)$ is defined as in (3). The Fourier transform of (7) yields

$$(\omega_+^2 - k^2 V^2) \hat{\varepsilon}_+ + (\omega_-^2 - k^2 V^2) \hat{\varepsilon}_- = \frac{\omega_-^2 - \omega_+^2}{ik} (\varepsilon_+ - \varepsilon_-), \quad (8)$$

where $\hat{\varepsilon}^\pm(k) = \int_{-\infty}^{\infty} \varepsilon(\eta) H(\pm\eta) e^{ik\eta} d\eta$, and we introduced the notation $\varepsilon_* = \sigma_0/(\gamma^2 - 1)$. Although the dispersion relations in the D problem $\omega_\pm^2(k) = \omega_\pm^2(k)/\gamma^2 = 4 \sin^2(k/2)$ are more complex than in the QC problem, the latter qualitatively captures the long-wave behavior, as can be seen in Fig. 4. More precisely, the QC model operates with only four approximate nonzero roots in the D problem that are closest to the origin [36].

Eq. (8) can be solved by the Wiener-Hopf technique, and the solution once again takes the form of Eq. (4) that includes radiative ($\Lambda_\pm(\eta)$) and exponentially localized ($\Phi_\pm(\eta)$) components; see [41] for the details. In the generic case admissible subkink and shock solutions feature a single radiation mode (5) propagating behind the front, where the wave number k^- is now the positive root of the characteristic equation $\omega_-(k) = Vk$ for the D problem, while $\Lambda_+ \equiv 0$. In the superkink case, $\Lambda_\pm \equiv 0$. For both types of kinks, the limiting states are fully determined by V via

$$\varepsilon_\pm = \varepsilon_* + \frac{\varepsilon_c - \varepsilon_*}{R} \left(\frac{1 - V^2}{\gamma^2 - V^2} \right)^{\mp 1/2},$$

where $R = 1$ for superkinks and $R = k^-/k^+$ for subkinks. In the case of shocks one of the limiting states remains a free parameter, which agrees with both continuum and QC approximations. The admissibility diagram for the D model is similar to the one shown in Fig. 6 for the QC model [41].

To conclude, we presented the framework revealing the intricate relations between various classes of transition fronts in non-integrable FPU system. To achieve analytical transparency, we constructed a minimal QC model based on the higher order approximation of the kinetic energy. Comparison with the exact solution of the FPU system shows that the chosen approximation adequately describes the complex interrelation between different types of transition fronts. The obtained front solutions can be interpreted as microscopic descriptions of Whitham shocks [45, 46]. They correspond to heteroclinic traveling waves of the original dispersive model that can connect not only critical points but also *periodic orbits*. To capture such connections, a higher order QC model is necessary, and the ensuing rich variety of transition fronts can be attributed to degrees of freedom brought by higher order QC approximation of FPU. To build bridges between different types of transition fronts we draw upon different physical considerations, including characteristics, barriers, critical manifolds and kinetic relations, which all point to the existence of exactly *three* universality classes of transition fronts.

Acknowledgments. The authors thank G. Mishuris for helpful discussions. The work of AV was supported by the NSF grant DMS-1808956. LT and NG acknowledge the support of the French Agence Nationale de la Recherche under the grant ANR-17-CE08-0047-02.

-
- [1] S. Kamvissis, *Physica D* **65**, 242 (1993).
- [2] B. Holian and G. Straub, *Phys. Rev. B* **18**, 1593 (1978).
- [3] N. Flytzanis, S. Pnevmatikos, and M. Remoissenet, *J. Phys. C* **18**, 4603 (1985).
- [4] M. Peyrard, S. Pnevmatikos, and N. Flytzanis, *Physica D* **19**, 268 (1986).
- [5] B. Deng, P. Wang, V. Tournat, and K. Bertoldi, *J. Mech. Phys. Solids* **136**, 103661 (2020).
- [6] N. K. Lowman and M. A. Hoefer, *Phys. Rev. A* **88**, 013605 (2013).
- [7] B. Hayes and M. Shearer, *Proc. Royal Soc. Edinburgh A* **129**, 733 (1999).
- [8] X. An, T. R. Marchant, and N. F. Smyth, *Proc. Royal Soc. A* **474**, 20180278 (2018).
- [9] H. Yasuda, C. Chong, J. Yang, and P. Kevrekidis, *Phys. Rev. E* **95**, 062216 (2017).
- [10] A. Vattré and C. Denoual, *J. Mech. Phys. Solids* **131**, 387 (2019).
- [11] S. Baqer and N. F. Smyth, *Physica D* **403**, 132334 (2020).
- [12] H. Yasuda, L. Korpas, and J. Raney, *Phys. Rev. Appl.* **13**, 054067 (2020).
- [13] J. R. Raney, N. Nadkarni, C. Daraio, D. M. Kochmann, J. A. Lewis, and K. Bertoldi, *Proc. Nat. Acad. Sci.* **113**, 9722 (2016).
- [14] D. M. Kochmann and K. Bertoldi, *Appl. Mech. Rev.* **69** (2017).
- [15] Y. Zhang, B. Li, Q. Zheng, G. M. Genin, and C. Chen, *Nat. Comm.* **10**, 1 (2019).
- [16] M. Sato, B. Hubbard, and A. Sievers, *Rev. Modern Phys.* **78**, 137 (2006).
- [17] N. Nadkarni, A. F. Arrieta, C. Chong, D. M. Kochmann, and C. Daraio, *Phys. Rev. Lett.* **116**, 244501 (2016).
- [18] N. Nadkarni, C. Daraio, and D. M. Kochmann, *Phys. Rev. E* **90**, 023204 (2014).
- [19] D. S. Ricketts and D. Ham, *Electrical solitons: theory, design, and applications* (CRC Press, 2018).
- [20] D. Chevriaux, R. Khomeriki, and J. Leon, *Phys. Rev. B* **73**, 214516 (2006).
- [21] M. E. Mossman, M. A. Hoefer, K. Julien, P. G. Kevrekidis, and P. Engels, *Nat. Comm.* **9**, 1 (2018).
- [22] S. Peotta and M. Di Ventra, *Phys. Rev. A* **89**, 013621 (2014).
- [23] E. Bettelheim, A. G. Abanov, and P. Wiegmann, *Phys. Rev. Lett.* **97**, 246401 (2006).
- [24] E. Fermi, P. Pasta, and S. Ulam, *Studies of the nonlinear problems*, Tech. Rep. (Los Alamos Sci. Lab., NM, 1955).
- [25] G. Gallavotti, *The Fermi-Pasta-Ulam problem: a status report*, Vol. 728 (Springer, 2007).
- [26] L. Truskinovskii, *J. Appl. Math. Mech.* **51**, 777 (1987).
- [27] E. Trofimov and A. Vainchtein, *Cont. Mech. Thermodyn.* **22**, 317 (2010), Erratum, *Ibid.* **25**: 107-108, 2013.
- [28] L. Truskinovsky, in *Shock induced transitions and phase structures in general media* (Springer, 1993) pp. 185–229.
- [29] N. Gorbushin and L. Truskinovsky, *Phil. Trans. Royal Soc. A* **378**, 20190115 (2020).
- [30] W. Atkinson and N. Cabrera, *Phys. Rev.* **138**, A763 (1965).
- [31] L. Truskinovsky and A. Vainchtein, *SIAM J. Appl. Math.* **66**, 533 (2005).
- [32] L. I. Slepyan, *Models and phenomena in fracture mechanics* (Springer Science & Business Media, 2012).
- [33] M. Charlotte and L. Truskinovsky, *J. Mech. Phys. Solids* **60**, 1508 (2012).
- [34] L. I. Slepyan and L. V. Troyankina, *J. Appl. Mech. Tech. Phys.* **25**, 921 (1984).
- [35] G. Iooss, *Nonlinearity* **13**, 849 (2000).
- [36] L. Truskinovsky and A. Vainchtein, *Cont. Mech. Thermodyn.* **18**, 1 (2006).
- [37] C. I. Christov, G. A. Maugin, and A. V. Porubov, *C. R. Mécanique* **335**, 521 (2007).
- [38] P. Rosenau, *Phys. Lett. A* **118**, 222 (1986).
- [39] P. Rosenau and S. Schochet, *Chaos* **15**, 015111 (2005).
- [40] I. M. Gelfand and S. V. Fomin, *Calculus of Variations* (Prentice-Hall, Englewood Cliffs, NJ, 1963).
- [41] See Supplemental Material at [URL will be inserted by publisher] for [give brief description of material].
- [42] L. M. Truskinovskii, in *Dokl. Akad. Nauk*, Vol. 265 (Russian Academy of Sciences, 1982) pp. 306–310.
- [43] L. Truskinovsky, in *Dynamics of Crystal Surfaces and Interfaces* (Springer, 2002) pp. 185–197.
- [44] B. L. Holian, *Shock waves* **5**, 149 (1995).
- [45] P. Sprenger and M. A. Hoefer, *Nonlinearity* **33**, 3268 (2020).
- [46] S. Gavriluk, B. Nkonga, K.-M. Shyue, and L. Truskinovsky, *Nonlinearity* **33**, 5477 (2020).

Universality classes of transition fronts in the FPU model: Supplementary Material

N.Gorbushin,¹ A. Vainchtein,² and L. Truskinovsky¹

¹PMMH, CNRS – UMR 7636, CNRS, ESPCI Paris, PSL Research University, 10 rue Vauquelin, 75005 Paris, France

²Department of Mathematics, University of Pittsburgh, Pittsburgh, Pennsylvania 15260, USA

(Dated: April 13, 2021)

a. D model: numerical simulations We solved the FPU system numerically using Runge-Kutta method (algorithm ode45 from Matlab) on a finite lattice of $N = 1000$ springs with Riemann initial conditions

$$\varepsilon_n(0) = \begin{cases} \varepsilon_l, & n < 500, \\ 0, & n \geq 500, \end{cases} \quad \frac{d\varepsilon_n}{dt}(0) = 0$$

and free boundary conditions. The duration of simulation was chosen to prevent any boundary effects on the front dynamics.

In each simulation we varied ε_l and $\Delta\sigma = \sigma_0 - (E_2 - E_1)\varepsilon_c$, while keeping all other parameters fixed. As described in the main text, we found that depending on these two varied parameters, four types of transition fronts form (subkinks, stationary shocks, dispersive shocks waves and superkinks). In particular, we found that superkinks ($c_1 < V < c_2$) can only appear if $\Delta\sigma < -\varepsilon_c(E_2 - E_1) < 0$.

b. QC model: explicit solution The structure of solution of the QC model is determined by the roots of the characteristic equations $\omega_{\pm}^2(k) - V^2k^2 = 0$. Due to the symmetry of the functions involved it suffices to seek nonzero roots with $\Im k > 0$ and $\Re k > 0$. There is also a double root at $k = 0$, providing a linear contribution to the solution with only a constant term ultimately entering due to the assumption of boundedness. The nonzero roots $k_{\pm}^{(j)}$, $j = 1, 2, 3, 4$ possess the symmetry $k_{\pm}^{(3)} = -k_{\pm}^{(1)}$ and $k_{\pm}^{(4)} = -k_{\pm}^{(2)}$. The analysis of the remaining algebraic problem shows that

$$\begin{aligned} k_+^{(1)} &= ip, & k_+^{(2)} &= s, & V < 1, \\ k_+^{(1,2)} &= ip_{1,2}, & 1 < V < V_*, \\ k_+^{(1,2)} &= id \pm f, & V > V_* \end{aligned} \quad (1)$$

and

$$\begin{aligned} k_-^{(1)} &= iq, & k_-^{(2)} &= r, & V < \gamma, \\ k_-^{(1,2)} &= iq_{1,2}, & \gamma < V < V_{**}, \\ k_-^{(1,2)} &= ig \pm w, & V > V_{**}, \end{aligned} \quad (2)$$

where $V_* = \sqrt{12/7}$, $V_{**} = \gamma\sqrt{12/7} > V_*$, and $p, s, p_{1,2}, d, f, q, r, q_{1,2}, g$ and w are explicitly known real and positive functions of V .

For subkinks ($V < 1$), the solution takes the form

$$\varepsilon(\eta) = \begin{cases} \varepsilon_- + B_1 e^{q\eta} + B_2 \cos(r\eta) + B_3 \sin(r\eta), & \eta < 0 \\ \varepsilon_+ + A_1 e^{-p\eta}, & \eta > 0, \end{cases} \quad (3)$$

where we have applied the radiation and boundary conditions. The consistency condition yields $\varepsilon_+ + A_1 = \varepsilon_c$ and $\varepsilon_- + B_1 +$

$B_2 = \varepsilon_c$. Together with the remaining jump conditions this yields the following linear system for the coefficients in (3):

$$\begin{aligned} -C_0 A_1 + B_1 + B_2 &= b \\ pA_1 + qB_1 + rB_3 &= 0, \\ p^2 A_1 - q^2 B_1 + r^2 B_2 &= 0, \\ p^3 A_1 + q^3 B_1 - r^3 B_3 &= 0, \end{aligned}$$

where

$$C_0 = \frac{V^2 - 1}{V^2 - \gamma^2}, \quad b = (1 - C_0)\varepsilon_c + \frac{\sigma_0}{V^2 - \gamma^2}.$$

For $V > 1$ the structure of the roots in (1) and (2) changes depending on the value of V relative to the thresholds V_* and V_{**} , the existence of which is an artifact of the QC approximation. To account for this, it is convenient to introduce

$$\lambda_{1,2} = \begin{cases} -p_{1,2}, & 1 < V < V_* \\ -d \pm if, & V > V_* \end{cases}$$

and

$$\mu_{1,2} = \begin{cases} q_{1,2}, & \gamma < V < V_{**} \\ g \pm iw, & V > V_{**}. \end{cases}$$

Then for shocks ($1 < V < \gamma$) we have

$$\varepsilon(\eta) = \begin{cases} \varepsilon_- + B_1 e^{q\eta} + B_2 \cos(r\eta) + B_3 \sin(r\eta), & \eta < 0 \\ \varepsilon_+ + A_1 e^{\lambda_1 \eta} + A_2 e^{\lambda_2 \eta}, & \eta > 0. \end{cases} \quad (4)$$

The consistency condition yields $\varepsilon_+ + A_1 + A_2 = \varepsilon_c$ and $\varepsilon_- + B_1 + B_2 = \varepsilon_c$, and the linear system for the coefficients in (4) becomes

$$\begin{aligned} -C_0(A_1 + A_2) + B_1 + B_2 &= b \\ \lambda_1 A_1 + \lambda_2 A_2 - qB_1 - rB_3 &= 0, \\ \lambda_1^2 A_1 + \lambda_2^2 A_2 - q^2 B_1 + r^2 B_2 &= 0, \\ \lambda_1^3 A_1 + \lambda_2^3 A_2 - q^3 B_1 + r^3 B_3 &= 0. \end{aligned} \quad (5)$$

This system of four equations does not allow one to find all five unknown coefficients, which means that the structure of shocks is not fully determined internally. The solution will be fully defined if we provide an additional condition, for instance, $\varepsilon_+ = 0$, which means that $A_1 + A_2 = \varepsilon_c$.

Finally, in the range $V > \gamma$ the solution reads

$$\varepsilon(\eta) = \begin{cases} \varepsilon_- + B_1 e^{\mu_1 \eta} + B_2 e^{\mu_2 \eta}, & \eta < 0 \\ \varepsilon_+ + A_1 e^{\lambda_1 \eta} + A_2 e^{\lambda_2 \eta}, & \eta > 0, \end{cases} \quad (6)$$

where $\varepsilon_+ + A_1 + A_2 = \varepsilon_c$, $\varepsilon_- + B_1 + B_2 = \varepsilon_c$, and the coefficients can be found explicitly by solving the linear system

$$\begin{aligned} -C_0(A_1 + A_2) + B_1 + B_2 &= b, \\ \lambda_1 A_1 + \lambda_2 A_2 - \mu_1 B_1 - \mu_2 B_2 &= 0, \\ \lambda_1^2 A_1 + \lambda_2^2 A_2 - \mu_1^2 B_1 - \mu_2^2 B_2 &= 0, \\ \lambda_1^3 A_1 + \lambda_2^3 A_2 - \mu_1^3 B_1 - \mu_2^3 B_2 &= 0. \end{aligned}$$

To check numerical stability of the obtained solutions we also performed direct numerical simulations of an initial value problem. We used a finite domain $x \in (0, H)$, where $H = 200$, and adopted the Riemann initial conditions:

$$\varepsilon(x, 0) = \begin{cases} \varepsilon_l, & x < H/2, \\ 0, & x \geq H/2, \end{cases} \quad \frac{\partial \varepsilon}{\partial t}(x, 0) = 0.$$

We set first and second spatial derivatives to zero at the boundaries and used the finite-difference method detailed in [1].

Fig. 1 shows the results of the simulations, where we fix $\varepsilon_r = 0$ and vary ε_l and $\Delta\sigma$. As in D problem discussed in the

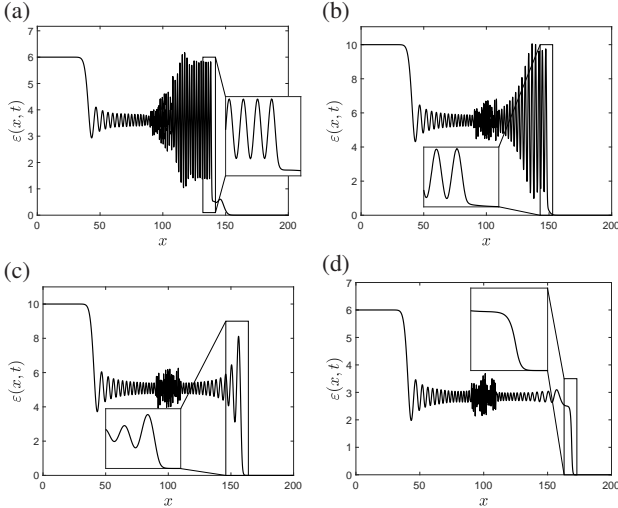


Figure 1. Different regimes of front propagation when $E_1 = 1$, $E_2 = 1.5$, $\rho = 1$, $\varepsilon_c = 1$ and $h = 1$ at $t = 50$: (a) subkink ($\varepsilon_l = 6$, $\Delta\sigma = 2.5$); (b) conventional shock ($\varepsilon_l = 10$, $\Delta\sigma = 2.5$); (c) dispersive shock ($\varepsilon_l = 10$, $\Delta\sigma = 0$); (d) superkink ($\varepsilon_l = 6$, $\Delta\sigma = -1.5$).

main text, we see the formation of subkinks, conventional and dispersive shocks and superkinks, depending on the choice of $\Delta\sigma$ and ε_l .

c. Discrete (D) model: explicit solution Up to a common constant, represented in the Fourier space by a delta function, the function $\hat{\varepsilon}(k) = \hat{\varepsilon}^+(k) + \hat{\varepsilon}^-(k)$ can be written as a sum of the general solution $\hat{\chi}^\pm(k)$ of the homogeneous problem and a particular solution $\hat{\chi}_0^\pm(k)$ of the inhomogeneous problem, which accounts for the boundary conditions. Then in the Fourier space the D problem reduces to

$$\begin{aligned} L(k) [\hat{\chi}^+(k) + \hat{\chi}_0^+(k)] + [\hat{\chi}^-(k) + \hat{\chi}_0^-(k)] \\ = (1 - L(k))/(ik) (\varepsilon_+ - \varepsilon_*), \end{aligned} \quad (7)$$

where $L(k) = L_+(k)/L_-(k)$, $L_\pm(k) = (\omega_\pm^2(k) + (0 + ikV)^2)$, with $0 \pm ikV = \lim_{s \rightarrow 0^+} (s \pm ikV)$.

A particular solution can be represented as a sum of functions belonging to the null spaces of the operators $L_\pm(k)$:

$$L_+(k)\hat{f}_+(k) = 0, \quad L_-(k)\hat{f}_-(k) = 0. \quad (8)$$

In what follows, we consider the generic case when V is non-resonant ($V \neq \omega'_+(k)$ and $V \neq \omega'_-(k)$ for any real k). We define the sets $\mathcal{Z} = \mathcal{Z}_r^+ \cup \mathcal{Z}_r^- \cup \mathcal{Z}_c^+ \cup \mathcal{Z}_c^-$ and $\mathcal{P} = \mathcal{P}_r^+ \cup \mathcal{P}_r^- \cup \mathcal{P}_c^+ \cup \mathcal{P}_c^-$ of nonzero roots, where

$$\begin{aligned} \mathcal{Z}_r^\pm &= \{z : L_\pm(z) = 0, z \neq 0, \Im z = 0, \omega'_\pm(z) \gtrless V\}, \\ \mathcal{P}_r^\pm &= \{p : L_\pm(p) = 0, p \neq 0, \Im p = 0, \omega'_\pm(p) \gtrless V\}, \\ \mathcal{Z}_c^\pm &= \{z : L_\pm(z) = 0, \Im z \gtrless 0\}, \\ \mathcal{P}_c^\pm &= \{p : L_\pm(p) = 0, \Im p \gtrless 0\}. \end{aligned} \quad (9)$$

Then solutions of (8) can be written in the form

$$\begin{aligned} \hat{f}_+(k) &= 2\pi[A_+\delta(k) + iB_+\delta'(k)] + \sum_{k_j \in \mathcal{Z}} C_j^{(+)}\delta(k - k_j), \\ \hat{f}_-(k) &= 2\pi[A_-\delta(k) + iB_-\delta'(k)] + \sum_{k_j \in \mathcal{P}} C_j^{(-)}\delta(k - k_j). \end{aligned}$$

The first two terms in both expressions correspond to double zeroes of $L_\pm(k)$ at $k = 0$ and describe linear functions $f_\pm(\eta) = A_\pm + B_\pm\eta$ in the physical space. Since solutions must be bounded, we set $B_\pm = 0$. In addition, since the boundary conditions are of long-wave type, we have $C_j^{(\pm)} = 0$. Given that $2\pi\delta(k) = 1/(0 - ik) + 1/(0 + ik)$, we have

$$\hat{\chi}_0^\pm(k) = \frac{\varepsilon_\pm}{0 \mp ik}, \quad (10)$$

where we used the fact that $\langle \varepsilon(\eta) \rangle \rightarrow \varepsilon_\pm$ at $\eta \rightarrow \pm\infty$ and set $A_\pm = \varepsilon_\pm$.

To find the general solution $\hat{\chi}^\pm(k)$ of the homogeneous equation, we use the Wiener-Hopf technique [2–4]. It requires the elimination of the singularity at zero on both sides of the equation and is based on the factorizing the kernel function in the form $L(k) = L^+(k)L^-(k)$, where the superscripts \pm specify functions that are analytic in $\Im k \gtrless 0$, respectively (here $L^\pm(k)$ should not be confused with $L_\pm(k)$ denoting the characteristic functions ahead and behind the front). If we divide (7) by $L^-(k)$ and multiply by ik , to remove a singularity at $k = 0$, we obtain

$$\begin{aligned} L^+(k) [-\varepsilon_* - ik(\hat{\chi}^+(k) + \hat{\chi}_0^+(k))] \\ = \frac{1}{L^-(k)} [ik(\hat{\chi}^-(k) + \hat{\chi}_0^-(k)) + \varepsilon_*]. \end{aligned} \quad (11)$$

Using $L(0) = (1 - V^2)/(\gamma^2 - V^2)$, $L(-k) = \overline{L(k)}$ and the fact that $L(k) \sim 1$ when $k \rightarrow \infty$, we can write $L^\pm(k) = \exp\left(\pm \frac{1}{2\pi i} \int_{-\infty}^{\infty} \frac{\text{Log}L(\xi)}{\xi - k} d\xi\right)$, where $\text{Log}(z)$ is a principal value of the logarithm. The functions $L^\pm(k)$ are free of zeros and poles in their domains of analyticity and can

be further factorized as $L^\pm(k) = l^\pm(k)L_0^\pm(k)$, where the first and second factors involve real and non-real roots of the characteristic equations, respectively.

More specifically, consider the sets $\mathcal{Z}_r^+ \cup \mathcal{Z}_r^-$ and $\mathcal{P}_r^+ \cup \mathcal{P}_r^-$ of nonzero real roots defined in (9). These roots correspond to radiated lattice waves; due to the symmetry about the origin, it suffices to only consider positive roots. When the sets are nonempty for given V , they contain an odd number of positive real roots, given by $2l + 1$ and $2m + 1$, respectively. We arrange these roots in the ascending order: $z_j < z_{j+1}$, $j = 1, \dots, 2l$, and $p_j < p_{j+1}$, $j = 1, \dots, 2m$. Applying the radiation condition, one can show that the function $l^-(k)$ should contain zeros z_{2j-1} , $j = 1, \dots, l + 1$ and poles p_{2j-1} , $j = 1, \dots, m + 1$, with the odd indices that belong to the sets \mathcal{Z}_r^- and \mathcal{P}_r^- in (9), respectively, whereas the remaining zeroes, z_{2j} , $j = 1, \dots, l$, and poles, p_{2j} , $j = 1, \dots, m$, contribute to $l^+(k)$ and are contained in \mathcal{Z}_r^+ and \mathcal{P}_r^+ , respectively. Physically, this ensures that the radiated waves carry the energy away from the front.

Next, we note that in the case of superkinks ($V > \gamma$) both functions $L_\pm(k)$ have no nonzero real roots (and hence no radiated waves). For shocks ($1 < V < \gamma$) only $L_-(k)$ has such roots, with $m = 0$ for V below the first resonance velocity $V_1 > 1$ such that $\omega_2'(k) = V_1 k$ for some real k , $m = 1$ for V between the first and second resonance velocities, etc. Finally, for subkinks ($V < 1$) each of the characteristic equations has at least one positive real root, with l and m each increasing by one when the corresponding resonance velocity is crossed. In view of this, we have

$$l^\pm(k) = \begin{cases} R^{\pm 1}, & V < 1 \text{ or } V > \gamma, \\ iR^{\pm 1}(0 \mp ik)^{\pm 1}, & 1 < V < \gamma, \end{cases} \quad (12)$$

where $R = (\prod_{j=1}^l z_{2j} \prod_{j=1}^{m+1} p_{2j-1}) / (\prod_{j=1}^{l+1} z_{2j-1} \prod_{j=1}^m p_{2j})$ for subkinks ($V < 1$) and $R = (\prod_{j=1}^{m+1} p_{2j-1}) / (\prod_{j=1}^m p_{2j})$ for shocks ($1 < V < \gamma$), while for superkinks the absence of radiation implies $R = 1$.

We now consider the asymptotic behavior of the functions $L^\pm(k)$. Depending on the type of the front we obtain

$$L^\pm(k) = \begin{cases} \sqrt{\frac{1-V^2}{\gamma^2-V^2}} + O(k), & k \rightarrow 0, \\ V < 1 \text{ or } V > \gamma, \\ i\sqrt{\frac{V^2-1}{\gamma^2-V^2}} + O(k), & k \rightarrow 0, \\ 1 < V < \gamma \end{cases} \quad (13)$$

and

$$L^\pm(k) = \begin{cases} R^{\mp 1} + O\left(\frac{1}{k}\right), & k \rightarrow \infty, \\ V < 1 \text{ or } V > \gamma, \\ R^{\mp 1} k^{\pm 1} + O(k^{-1 \pm 1}), & k \rightarrow \infty, \\ 1 < V < \gamma \end{cases} \quad (14)$$

One can also show that near the real singularities

$$\frac{1}{L^+(k)} = \frac{\omega_2(z_{2j}) - (z_{2j}V)^2}{2z_{2j}Vi|\omega_2'(z_{2j}) - V|} L^-(z_{2j}) \frac{1}{0 - i(k - z_{2j})}, \quad k \rightarrow z_{2j},$$

and

$$L^-(k) = \frac{\omega_1(p_{2j-1}) - (p_{2j-1}V)^2}{2p_{2j-1}Vi|\omega_1'(p_{2j-1}) - V|} \times \frac{1}{L^+(p_{2j-1})} \frac{1}{0 + i(k - p_{2j-1})}, \quad k \rightarrow p_{2j-1},$$

with similar expressions for the negative real singular points.

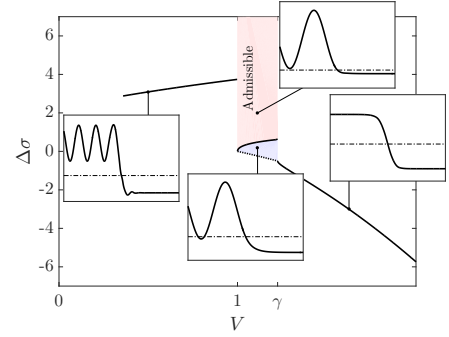


Figure 2. Admissibility sets of solutions of the D problem. In the blue region we observe $\varepsilon(\eta) \leq \varepsilon_c$ when $\eta < \varepsilon_c$, and the dashed lower boundary of the region marks the threshold $\varepsilon_- = \varepsilon_c$. The insets show examples of the strains $\varepsilon(\eta)$. Here $\gamma^2 = 1.5$, $\varepsilon_c = 1$, and we set $\varepsilon_+ = 0$ for shock solutions. The corresponding diagram for the QC problem is shown in the main text; the two diagrams differ significantly only at small $V < 1$, where the QC model, as expected, does not capture the inadmissibility of slow subkink solutions.

Using the asymptotic estimates (14) at $k \rightarrow \infty$, recalling (11), (10) and applying the Liouville theorem, we conclude that

$$L^+(k) \left[-\varepsilon_* - ik \left(\hat{\chi}^+(k) + \frac{\varepsilon_+}{0 - ik} \right) \right] = \frac{1}{L^-(k)} \left[-\varepsilon_* + ik \left(\hat{\chi}^-(k) + \frac{\varepsilon_-}{0 + ik} \right) \right] = M(k), \quad (15)$$

where $M(k) = \psi_0 + \psi_1 k$. By (14), both sides of (15) are constant at infinity when $V < 1$ or $V > \gamma$. Therefore, we must set $\psi_1 = 0$ for these velocity ranges. The solution in the Fourier space is

$$\hat{\chi}^\pm(k) = \frac{\varepsilon_* - \varepsilon_\pm}{0 \mp ik} + \frac{\psi_0 + \psi_1 k}{0 \mp ik} [L^\pm(k)]^{\mp 1}. \quad (16)$$

Inverting this relations, we can reconstruct the strains in the physical space:

$$\varepsilon(\eta) = \varepsilon_\mp + \frac{1}{2\pi} \int_{-\infty}^{\infty} \hat{\chi}^\mp(k) e^{-ik\eta} dk, \quad \eta \leq 0. \quad (17)$$

Using (16) and recalling the asymptotic behavior of the $L^\pm(k)$ in (13) and (14), we can determine the constants ψ_0 and ψ_1 ,

keeping in mind that $\psi_1 = 0$ in the subkink and superkink regimes, as noted above. For subkinks ($V < 1$) and superkinks ($V > \gamma$), this yields $\psi_0 = (1/R)(\varepsilon_c - \varepsilon_*)$. Then the equilibrium states are

$$\varepsilon_{\pm} = \varepsilon_* + \frac{\varepsilon_c - \varepsilon_*}{R} \left(\frac{1 - V^2}{\gamma^2 - V^2} \right)^{\mp 1/2}. \quad (18)$$

For the shocks ($1 < V < \gamma$) we obtain instead

$$\psi_0 = i \sqrt{\frac{\gamma^2 - V^2}{1 - V^2}} (\varepsilon_- - \varepsilon_*), \quad \psi_1 = \frac{\varepsilon_c - \varepsilon_*}{R},$$

Thus, although in all three cases we have $\varepsilon_- = L(0)(\varepsilon_+ - \varepsilon_*) + \varepsilon_*$, which is equivalent to the RH condition $V^2 = [\sigma(\varepsilon_+) - \sigma(\varepsilon_-)]/(\varepsilon_+ - \varepsilon_-)$, in the case of shocks the limiting states ε_{\pm} are *not* uniquely determined by V , i.e. there is no condition equivalent to (18) we have for subkinks and superkinks, and one of these variables is prescribed independently.

The solution (17) in all three cases can be expressed in the form $\varepsilon(\eta) = \varepsilon_{\mp} + \Lambda_{\mp}(\eta) + \Phi_{\mp}(\eta)$, $\eta \leq 0$. Here $\Phi_{\mp}(\eta)$ are exponentially decaying functions given by the infinite sums over the non-real roots defined in (9):

$$\begin{aligned} \Phi_-(\eta) &= \sum_{p \in \mathcal{P}_c^-} \frac{\omega_1^2(p) - (pV)^2}{2p^2V(\omega_2'(p) - V)} \frac{(\psi_0 + \psi_1 p)}{L^+(p)} e^{ip\eta} \\ \Phi_+(\eta) &= \sum_{z \in \mathcal{Z}_c^+} \frac{\omega_2^2(z) - (zV)^2}{2z^2V(\omega_1'(z) - V)} L^-(z) (\psi_0 + \psi_1 z) e^{iz\eta}, \end{aligned}$$

where we recall (9), and $\Lambda_{\mp}(\eta)$ correspond to radiation. For subkinks ($V < 1$), we have

$$\begin{aligned} \Lambda_-(\eta) &= 2 \sum_{j=1}^{m+1} \alpha_j^- \cos(p_{2j-1}\eta + \beta_j^-), \\ \Lambda_+(\eta) &= 2 \sum_{j=1}^l \alpha_j^+ \cos(z_{2j}\eta + \beta_j^+), \end{aligned}$$

where the second sum is zero when $l = 0$. For shocks ($1 < V < \gamma$), there is no radiation ahead of the front, so $\Lambda_+(\eta) \equiv 0$, while the form of Λ_+ has the same form as above. The real coefficients α_j^{\pm} and β_j^{\pm} can be found using the polar representation of the complex numbers from

$$\begin{aligned} \alpha_j^- e^{-i\beta_j^-} &= \frac{L^+(p_{2j-1}) [\omega_1^2(p_{2j-1}) - (p_{2j-1}V)^2]}{2p_{2j-1}Vi [V - \omega_2'(p_{2j-1})]} \\ &\quad \times (\psi_0 + \psi_1 p_{2j-1}) \\ \alpha_j^+ e^{-i\beta_j^+} &= \frac{L^-(z_{2j}) [\omega_2^2(z_{2j}) - (z_{2j}V)^2]}{2z_{2j}Vi [\omega_1'(z_{2j}) - V]} (\psi_0 + \psi_1 z_{2j}), \end{aligned}$$

with the corresponding values of ψ_0 and ψ_1 ; only the first of these is relevant for shocks. Finally, for superkinks ($V > \gamma$) there is no radiation either ahead or behind the propagating front, and so in this case $\Lambda_-(\eta) = \Lambda_+(\eta) \equiv 0$.

The admissibility diagram for the D model is shown in Fig. 2.

[1] X. Wang and W. Dai, *Comp. Appl. Math.* **37**, 6560 (2018).

[2] L. I. Slepyan and L. V. Troyankina, *J. Appl. Mech. Tech. Phys.* **25**, 921 (1984).

[3] L. Slepyan, A. Cherkaev, and E. Cherkaev, *J. Mech. Phys. Solids* **53**, 407 (2005).

[4] E. Trofimov and A. Vainchtein, *Cont. Mech. Thermodyn.* **22**, 317 (2010), Erratum, *Ibid.* **25**: 107-108, 2013.